Optical and Quantum Electronics **25** *(1993) S569–S585*

Error-corrective optical neural networks modelled by persistent spectral hole-burning

O. OLLIKAINEN
Institute of Physics of the Estonian Academy of Sciences, 142 Riia Street, 202400 Tartu, Estonia

A. REBANE
Physical Chemistry Laboratory, Swiss Federal Institute of Technology, ETH-Zentrum, CH-8092 Zürich, Switzerland

K. K. REBANE
Institute of Physics of the Estonian Academy of Sciences, 142 Riia Street, 202400 Tartu, Estonia

Received 30 March; revised 30 November 1992; accepted 4 January 1993

We show that materials with the ability to form persistent spectral holes under illumination have frequency as an additional optically parallel accessible degree of freedom that may be incorporated into associative memory. This opens new possibilities for increasing the number of interconnections in optical models of neural networks. In our first example, a 144-element autoassociative memory matrix is constructed on two 12-bit vectors and has two dimensions (x and frequency ω). The probe vector at the memory input carries two erroneous bits (out of 12 bits) and is one-dimensional (spatial coordinate x); the memory output – with the error bits corrected – is one-dimensional in frequency ω. The second example uses memory input that is two-dimensional (image in coordinates x, y); the memory matrix is four-dimensional (x, y, ω, t), where t (time coordinate) is given by the temporal delay of photochemically accumulated stimulated photon echo signal; memory output is two-dimensional (ω and t) and corrects two bits out of the 12-bit vector. In the third example, quadratic autoassociative memory is coded in three dimensions (coordinates x, y, ω) and materializes $32 \times 32 \times 32 = 32\,768$ optical interconnections; the probe vector is given as a 32×32 spatial matrix (coordinates x, y); the output is one-dimensional, consists of 32 bits along the frequency axis, and corrects four erroneous bits.

1. Introduction

Persistent spectral hole-burning (PSHB) [1–3] provides a unique possibility for controlling by means of illumination with high spectral resolution such optical properties as the coefficient of absorption, and correlated to it (via Kramers–Kronig relations) index of refraction, in the impurity absorption band of doped solid materials.

0306–8919

Among the numerous applications of PSHB are high-resolution matrix spectroscopy of molecules (including chlorophyll and its relatives), narrowband wide-aperture optical spectral filters for transmission and modulation of light, high-sensitivity detection of deformation (strain) fields in solids, high-capacity optical memories and optical data processing, and time-and-space domain holography (see [3] and references therein).

The cornerstone of PSHB is the zero-phonon line (ZPL) in the impurity spectra of solids – the optical analogue of the Mössbauer resonance γ-line [4] (see also [5, 6] and references therein). ZPLs are not Doppler-broadened. At liquid-helium temperatures the ZPL of a single molecule (i.e. the homogeneous ZPL) has a very narrow width and very high peak intensity, which are close to the free atom's radiative values. For homogeneous ZPL widths, $\Gamma(T) \sim 10^{-2}$ to $10^{-4}\,\mathrm{cm}^{-1}$, the peak value of the absorption cross-section is

$$\sigma(T) = (\lambda^2/2\pi)F_{\mathrm{DW}}\Gamma(0)/\Gamma(T) = \sigma_{\mathrm{r}}\alpha(T)$$

where F_{DW} is the Debye–Waller factor, λ is the wavelength, and $\sigma_{\mathrm{r}} = \lambda^2/(2\pi)$ is the peak value of the absorption radiative cross-section. The temperature-dependent factor, $\alpha(T) = F_{\mathrm{DW}}\Gamma(0)/\Gamma(T)$, at liquid-helium temperatures may be estimated as $\alpha(T) \sim 0.1$ to 0.01 for a large variety of impurity doped solids; with increasing temperature it decreases rather rapidly. One of the finest and the most spectacular uses of the very high peak absorption cross-section of ZPLs at low temperatures is the recent development of spectroscopy of a single impurity molecule in solids [7–9].

For a body of molecules, ZPL as a noble spectral feature is strongly distorted by large inhomogeneous broadening: in the absorption and conventionally measured luminescence spectra of an impurity-doped medium, ZPLs form a wide band (up to 10^2 to $10^3\,\mathrm{cm}^{-1}$) comprising thousands of sharp resonances – the homogeneous ZPLs. Illumination with a narrow laser line produces spectrally selective interaction with that subset of impurity molecules whose ZPLs are in resonance with the laser's frequency. These impurity centres can undergo photostimulated changes, i.e. photochemical reaction (photoionization) in the molecule itself or any other irreversible process in the surrounding matrix. The outcome of such changes is usually alteration of the ZPL frequencies of the transformed impurity centres so that the new ZPL frequency (if there still is a ZPL) is far from the initial value. At the excitation laser frequency a hole (dip) is formed in the inhomogeneous band of impurity absorption. The hole width is given approximately by the convolution of the shapes of the laser line and ZPL homogeneous line, the hole area by the dose of illumination. A sharp spectral 'hole' is a negative image of the ZPL: it displays absence of ZPLs from the initial inhomogeneous ensemble (for features of hole-burning see, e.g., [10–12]).

Note that in all PSHB applications the light–matter interaction may be, and actually is, rather weak, i.e. no intense light for nonlinear optical field-strength-dependent effects is needed. The space- and frequency-domain pattern is created in PSHB material by accumulating changes of the coefficient of absorption and associated index of refraction under modest but sufficiently long-time illumination. Coherent time-domain optical responses such as photochemically accumulated stimulated photon echo [13], and the other PSHB effects arise from the circumstance that after hole-burning the optical characteristics of the material are changed. This difference between the properties of the material before and after the PSHB is caused by the change of the number of impurity molecules absorbing via their ZPLs at a given frequency ω. It should be also mentioned that in PSHB, because of the possibility of keeping excitation intensities low, the power broadening of ZPLs and, consequently, broadening of spectral holes may be avoided.

The theoretical upper limits for optical PSHB storage density are high. Optimistic estimates put them at 10^{12} bits cm^{-2} (i.e. 10^4 spectral holes per diffraction-limited spatial pixel of size $\lambda \times \lambda \sim 10^{-8}$ cm^2) or 10^{16} bits cm^{-3} for a volume storage memory (cell size $\lambda \times \lambda \times \lambda \sim 10^{-12}$ cm^3). Actually, the impurities interact with each other, e.g. energy transfer may take place. This results in perturbations of the ZPL distribution over frequencies and, consequently, in changes of the burnt-in hole profiles. In other words, this results in energy transfer and other cross-talk between spectral holes, and decreases the reliability of storage. Other reasons for erasing the hole structure (spectral diffusion) arise from changes of position or orientation of the atoms or molecules that constitute the host. The narrow width of ZPLs makes them sensitive to even the smallest changes of this kind. In disordered matrices (glasses, polymers), two-level systems contribute strongly. Interactions between the impurities can be suppressed by taking lower concentrations; however, this will result in a critical decrease of the average number of impurity molecules available to write a hole at a fixed wavelength at a fixed spatial spot. If we assume a concentration of impurities of 10^{18} molecules cm^{-3}, and storage density of 10^{16} bits cm^{-3}, there will be on average only 100 molecules to store one bit of information. Approximately the same average number of molecules is available in the three-dimensional storage scheme (two spatial coordinates and frequency) with storage density of 10^{12} bits cm^{-2}, because focusing of a laser beam to a diffraction-limited spot means concentrating light and burning holes within a cube of dimensions of λ^3, and the same amount of recording material per bit of information is available as in four-dimensional storage. This number is obviously too small: it is impossible to tell whether a difference of, say, 50 in impurity population after hole-burning between the two $\Delta x\,\Delta y\,\Delta z\,\Delta\omega$ cells is the result of PSHB or is just a statistical fluctuation. In the case of bit-by-bit storage we should be confident that the presence or absence of every one out of 10^{12} or more holes is fixed well beyond the influence of fluctuations in the number of impurities.

Distributed data storage, as is the case with holography and optical models of neural networks, considered below, therefore has certain advantages. The error-corrective capability of neural network models is also welcome.

This work has double motivation: first, to show that the error-corrective capabilities may be implemented optically by persistent spectral hole-burning. Second, to show that PSHB really can provide, in addition to the spatial coordinates (x, y, z), the frequency ω as a new dimension. If time-domain coherent recalls are used, time t also arises as a new coordinate for memory (photochemically accumulated stimulated photon echo is used and this, of course, also consumes frequency space). The possibility of fully parallel optical access to the stored data, even if the information is partially (or completely) coded in the frequency and/or time dimensions, makes the application of hole-burning materials for associative parallel processing especially attractive. This possibility has been demonstrated by reconstruction of full holographic spatial and also space- and time-domain images from input that is only a part of the image [14].

The remarkable property of associative memories is that the input information can include errors (e.g. probe images with erroneous elements) without loss of essential information: the recall automatically corrects for the errors towards the closest matching among the memorized information units. By arranging feedback (i.e. the output is fed back into the input) multistep corrections can be obtained.

Optical realizations of associative memories [15] exploit the additional possibilities that optics has in comparison to electronic devices, particularly these in massive matrix–matrix

multiplication procedures. In optical processors the matrices can be coded as spatial transparencies or holograms, and the multiplication procedure can be carried out simultaneously in many parallel channels. Conventional optics uses only the spatial (and polarization) degrees of freedom of the storage media, and, consequently, also of the optical signals. However, for processing of detailed image information a larger throughput capacity than is provided by conventional optical storage is needed. Also, for direct input/output of images in the two-dimensional format the optical multiplication process itself requires at least one more degree of freedom in addition to the three spatial coordinates.

Three examples are described in this paper. They differ by choice of coordinates, i.e. in the nature of the physical parameters used and measured, in the mathematical algorithms for constructing the memory matrix, and also in the number of bits processed.

2. Mathematical models

In digital autoassociative memories [16] data are usually presented as a set of M different vectors, $\boldsymbol{v}^{(s)}$ $(s = 1, \ldots, M)$, each vector being a sequence of N bits or elements. Various mathematical rules [17–19] can serve as algorithms to calculate from a given set of information vectors a corresponding memory or interconnections matrix, $\boldsymbol{T}$. Read-out of the memory gives an N-bit output vector, $\boldsymbol{v}^{(\mathrm{out})}$, which is constructed as a (thresholded) scalar product between the input (probe) vector, $\boldsymbol{v}^{(\mathrm{in})}$, and the memory matrix. The read-out procedure can be expressed mathematically as

$$\boldsymbol{v}^{(\mathrm{out})} = \mathrm{THR}\{\boldsymbol{T} \cdot \boldsymbol{v}^{(\mathrm{in})}\} \tag{1}$$

where THR{...} stands for the thresholding operation.

In our first two experiments we use an autoassociative memory algorithm (modified Hopfield neural network model) described in [18]. M two-dimensional information vectors, $v_{ij}^{(s)}$, $(i = 1, \ldots, P;\ j = 1, \ldots, R;\ s = 1, \ldots, M)$, consisting of elements 0 or 1, are memorized in a four-dimensional interconnection matrix. We use exactly this scheme in our second experiment. In the first experiment we consider a simplified version with only one-dimensional input and output, interconnected via a two-dimensional memory matrix. Actually, the same mathematical scheme is used, but there is only one index number which labels the vector elements $(i = 1, 2, \ldots, P + R)$, while the memory matrix elements are labelled by a double index $(i, j = 1, 2, \ldots, P + R)$ [20]. The mathematical prescription we use to calculate the elements of the memory is:

$$T_{ijkl} = T'_{ijkl} \Big/ \sum_{k,l=1}^{P,R} T'_{ijkl} \tag{2}$$

where

$$T'_{ijkl} = \begin{cases} T''_{ijkl}, & \text{if } T''_{ijkl} < 0 \\ 0, & \text{otherwise} \end{cases} \tag{3}$$

and

$$T''_{ijkl} = \begin{cases} \sum_{s=1}^{M} [2v_{ij}^{(s)} - 1][2v_{kl}^{(s)} - 1] & i, j \neq k, l \\ 0, & \text{if } i, j = k, l \end{cases} \tag{4}$$

Read-out of the memory by a probe vector $v^{(\mathrm{in})}$ is equal to the scalar product

$$v_{ij}^{(\mathrm{out})} = \mathrm{THR}\left\{ \sum_{k,l=1}^{P,R} T_{ijkl} v_{kl}^{(\mathrm{in})} \right\} \tag{5}$$

where THR{...} stands for the thresholding operator

$$\mathrm{THR}\{x\} = \begin{cases} 1, & \text{if } x \leq 0.5 \\ 0, & \text{otherwise} \end{cases} \tag{6}$$

In the development of Hopfield's model, higher-order associative memories have been suggested [21, 22]. In our third experiment we use quadratic associative memory or the so-called triple-correlation model. This model has been implemented using conventional holographic storage [18, 23]. According to the triple-correlation model, a set of M vectors comprising N elements each (values of elements 1 or 0) give a three-dimensional interconnection matrix with elements

$$T_{ijk} = \sum_{s=1}^{M} [2v_i^{(s)} - 1][2v_j^{(s)} - 1][2v_k^{(s)} - 1] + C \tag{7}$$

where $v_i^{(s)}$ is the ith element of the sth stored vector. A positive constant C is added in order to eliminate possible negative values of the tensor components. In this case optimum thresholding level depends on the composition of the probe vector, $v^{(\mathrm{in})}$, and is defined as

$$\mathrm{THR}\{x\} = \begin{cases} 1, & \text{if } x \geq CL^2 \\ 0, & \text{otherwise} \end{cases} \tag{8}$$

where L is the number of probe vector elements equal to 1. Read-out of the memory is equivalent to matrix–tensor scalar product:

$$v_i^{(\mathrm{out})} = \mathrm{THR}\left\{ \sum_{j,k=1}^{N} T_{ijk} v_j^{(\mathrm{in})} v_k^{(\mathrm{in})} \right\} \tag{9}$$

Note that in the present schemes we do not assume the output vector being directed once again back to the input of the memory. In our experiment the first pass of the processed signals through the memory already results in an error-free recollection of the data.

3. Experimental

Our PSHB material comprises two different organic impurity molecules (octaethylporphyrin and protoporphyrin) introduced into a polymeric matrix (polystyrene) at approximately equal concentrations of 10^{-3} to 10^{-4} mol^{-1}. The partially overlapping inhomogeneous absorption bands of the two impurities give in the 615 to 623 nm wavelength region a nearly 'flat' absorption frequency interval of width about 150 cm^{-1}, where the transmission of the sample (measured before the write-in exposures) varies between 1% and 2%. The spatial dimensions of the sample (block polystyrene) are 3×3 cm across and 4 mm in thickness. The sample is positioned inside an optical cryostat and immersed in liquid helium. At the working temperature of 2 K the narrowest hole-width is about 0.05 cm^{-1} for both types of impurities. The decay time of the written-in holes in this particular material has not been investigated. Our experiments show, however, that at 2 K this

decay is slow enough, since we do not notice any change in the hole structure in about 10 h waiting time (i.e. during the time when the cryostat boils empty of liquid helium).

As a laser source we use a picosecond Rhodamine 6G or DCM dye laser synchronously pumped by an 82-MHz mode-locked argon-ion laser (Spectra-Physics Model 4020). The frequency of the dye laser is tuned in steps within the 150 cm^{-1} spectral interval. To facilitate easy control over the dye laser frequency, we insert a thin etalon into the laser cavity in addition to the standard birefringent wavelength tuning element. Depending on the free spectral range of the etalon we have 10 to 40 fixed lasing frequencies within the 'flat' absorption range of the PSHB sample.

The quantum yield of the hole-burning process is about 1%. An average exposure energy of 1 to 10 mJ is required per cm^2 of the sample area, and cm^{-1} spectral interval, in order to increase the transmission of the sample at the illumination wavelength by a factor of 2. Note that as long as the homogeneous line width $\Gamma(T)$ is smaller than the laser line width, the necessary illumination dose decreases with the decreasing spectral width of the laser. In our experiments the writing intensity ranged at the sample from about 300 to 10 $\mu W\,cm^{-2}$. Depending on the line width of our dye laser, the exposure time per spectral hole (hologram) lasted from 10 to several hundreds of seconds. In the first two examples, 12 exposures are needed, and 32 in the third. The maximum total writing time needed to store the whole memory amounts then to approximately 30 min. The read-out of the information is performed at much lower intensity by attenuating the read beam with neutral-density filters. The attenuation is needed because the read-out illumination performs an additional PSHB that erases the information. A nondestructive read-out of the spectral holes and holograms could be secured using two-step absorption (photon-gated) PSHB materials [3, 9], which we did not apply here for considerations of simplicity.

The read-out is performed by collecting the transmitted (experiment 1) or the diffracted light (experiments 2 and 3) with a lens and by focusing it onto the detector. In experiments 1 and 3 the detector is a conventional photomultiplier. In experiment 2, where the temporal analysis of the photochemically accumulated stimulated photon echo (PASPE) signals is performed, the detector is a 20-ps time resolution synchroscan streak camera. The detection procedure per frequency interval is much faster than the write-in procedure and can be accomplished in a fraction of a second. Longer detection accumulation (averaging) times give better signal-to-noise ratio. More experimental details are given in [20, 24].

4. Results and discussion

4.1. First experiment

In the first example the memory matrix is materialized by using one spatial coordinate, x, and the frequency coordinate, ω. Along each coordinate 12 different values are distinguished. The 144-element memory matrix is calculated on the basis of the two 12-bit vectors,

$$\begin{aligned} v^{(1)} &= 100\ 101\ 101\ 001 \\ v^{(2)} &= 101\ 000\ 101\ 110 \end{aligned} \tag{10}$$

according to Equations 2 to 4, and is shown graphically in Fig. 1. In the experimental setup (Fig. 2) the variable x corresponds to 12 horizontal stripes arranged perpendicularly to the x-coordinate of the PSHB plate. The variable ω corresponds to 12 different

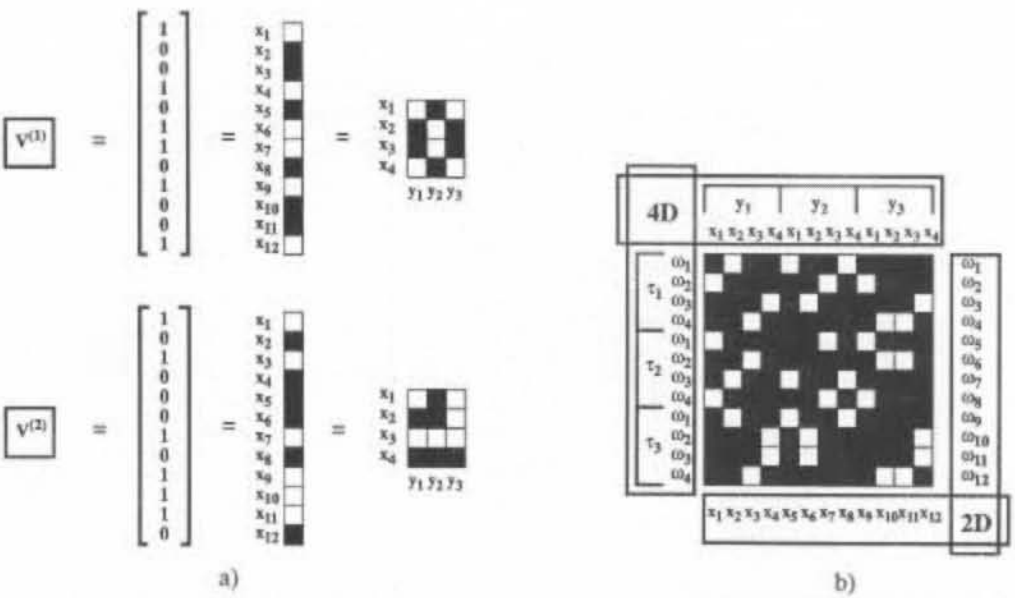

Figure 1 Information vectors and memory matrix in experiments 1 and 2. (a) Information vectors in one- and two-dimensional formats. (b) Memory matrix with two-dimensional partition (indices x_i and ω_j) and with four-dimensional partition (indices x_i, y_j, ω_k, τ_l); black squares correspond to zero elements, white squares correspond to nonzero elements.

frequencies at which holes can be burnt in the absorption spectrum.

To write-in the memory matrix we tune the laser sequentially to 12 different burn-in frequencies, ω_i. At each frequency the sample is exposed by directing the laser beam through a mask slide consisting of 12 horizontal stripes. Each stripe projects upon a corresponding section of the PSHB plate. If the calculated value of the memory matrix element T_{ij} is zero, then the jth stripe of the mask used for exposure at the ith frequency is opaque and no hole is burnt at the corresponding spatial and frequency element of the PSHB plate. Only if the memory matrix element T_{kl} is not zero (in our scheme, equal to 1), is the corresponding kth stripe of the mask for frequency l transparent, and a hole is burnt-in.

Once the memory is stored, it can be interrogated by an arbitrary 12-bit probe vector (elements 1 and 0). Probe vectors are coded as masks with corresponding transparent and opaque stripes in a way similar to that described above. A parallel beam of light comprising all the 12 frequencies is directed first through the probe mask and then through the PSHB sample so that each stripe of the mask projects at the corresponding section of the PSHB plate. Each of the 12 spatial elements of the input vector is connected to each of the 12 frequency-domain output vector elements via the 144 connections materialized by the PSHB plate. Consequently, the spatially integrated transmission of the probe mask along with the PSHB plate, measured at the 12 pre-fixed frequencies, implements the scalar vector–matrix product operation.

This measurement itself can be carried out either by using a broad spectral light source (e.g. glow lamp) and determining the relative transmission of the system at the pre-fixed frequencies, or, as is more convenient in the present experiment, by tuning the wavelength of the illuminating laser sequentially to the 12 frequencies involved. Figure 3 presents the

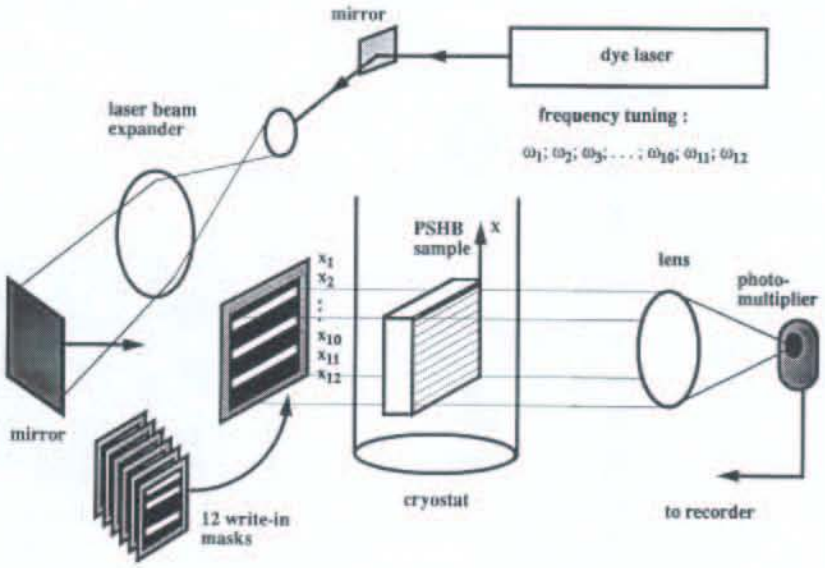

Figure 2 Setup of experiment 1.

relative transmission levels when the memory is illuminated through a mask that resembles one of the stored vectors – 10 out of 12 bits are the same as in $v^{(1)}$, two are different (erroneous). The corrected output vector is obtained after setting a common (inverting) threshold for the transmitted intensities (dashed line in Fig. 3). If the relative transmission signal at a given frequency is less than the thresholding level, then the corresponding bit value is set to 1; if the transmission is over the thresholding level, then the corresponding value is set to 0. The thresholded output is free of errors, i.e. it comprises exactly the same sequence of bits as the memorized vector, but the elements of the information vector are now labelled by frequency, not by the spatial coordinate as at the input. A signal coded in frequencies is preferable for transmission via optical fibres.

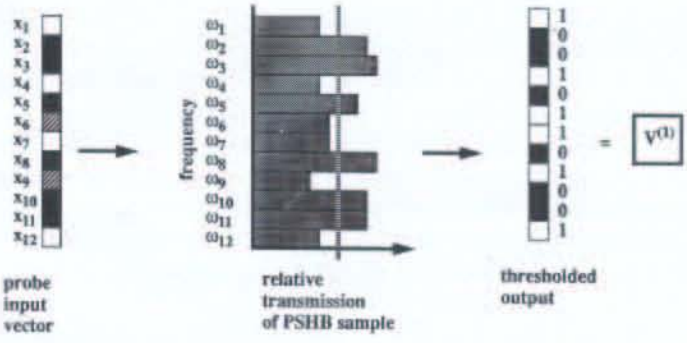

Figure 3 Results of experiment 1. The input probe vector comprises two error bits (shaded squares). The dashed line indicates the threshold level. Relative transmission signal above threshold level gives bit value 0, signal below threshold gives value 1. Thresholded memory output coincides with information vector $V^{(1)}$.

4.2. Second experiment

In the second example the memory T_{ijkl} is stored fully in accordance with prescription (2) to (4) by using four variables: two orthogonal spatial coordinates (x and y), frequency ω, and time delay τ. The spatial coordinates are labelled by indices i and j, frequency by index k, and time by index l. The indices i and k run from 1 to 4, j and l run from 1 to 3. The delay corresponds to a time-domain hologram PASPE signal. Two basic vectors are used. The content of the bits is the same as in example 1, but now they are arranged in a two-dimensional pattern. The 4D partition of the memory matrix is shown in Fig. 1b.

By formatting of the memory into a 4D matrix, and by coding input probe vectors in the x and y coordinates as two-dimensional images, the optical recall of the memory is also two-dimensional, coded in the frequency dimension ω and in the time dimension τ, and we can interpret the output signals directly as digital 2D images.

Figure 4a illustrates the setup for storing of the 4D memory. We apply the basic scheme of time- and space-domain hologram storage [13], which consists in illuminating the PSHB media with an object beam and time-delayed reference beam. The reference beam has a plane wavefront, and is spectrally broad enough to store in the time- and space-domain hologram signal pulses of 3 ps duration, each of which needs about $10\,\mathrm{cm}^{-1}$ of the frequency space. The reference beam uniformly illuminates the whole storage area of the PSHB sample. Spatial coding is carried out by using masks with 4×3 element binary patterns pre-calculated in accordance with Equations 2 to 4 positioned in the write-in object beam. The object beam is projected through the mask so that each spatial element of the mask coincides with the corresponding spatial element of the PSHB sample. The frequency coordinate corresponds to four different laser frequencies: ω_1, ω_2, ω_3, ω_4. At each frequency three PASPE holograms are stored, each using the same frequency interval but stored at a different delay value, τ, between the object and the reference beam ($\tau_1 = 40$ ps, $\tau_2 = 104$ ps, $\tau_3 = 180$ ps). The angle between the reference and the object beam is 6°.

Read-out of the memory is carried out by illuminating the hologram with the picosecond object beam (reference beam is blocked) through a two-dimensional (x, y) interrogating mask according to the scheme presented in Fig. 4b. The image pattern of the mask corresponds to an input vector with two error bits. At the output of the memory the diffracted holographic signal is focused onto the entrance slit of a streak camera. By the translation theorem of Fourier transforms, the time delay, τ, between the write-in signal and the reference pulse corresponds to multiplying the complex amplitude transmission coefficient of the time–space hologram by a factor of $\exp(\mathrm{i}\omega\tau)$. The corresponding distribution of intensities contains the factor $(1 - \cos\omega t)$, which is stored as modulation of the frequency spectrum of transparency of the PSHB sample. The hologram's time domain response to an interrogating pulse reproduces the value, τ, of the time delay [13]. Again, for experimental convenience, the recall of the hologram at different frequencies is measured sequentially by tuning the frequency of the illuminating picosecond laser. In principle, simultaneous time-resolved detection of all spectral components is also feasible. When arranged into a 4×3 matrix so that the vertical coordinate corresponds to the frequency (ω_1, ω_2, ω_3, ω_4) and the horizontal coordinate corresponds to the delay (τ_1, τ_2, τ_3) (Fig. 5), the resulting (thresholded) read-out data reproduces the corrected stored 2D image.

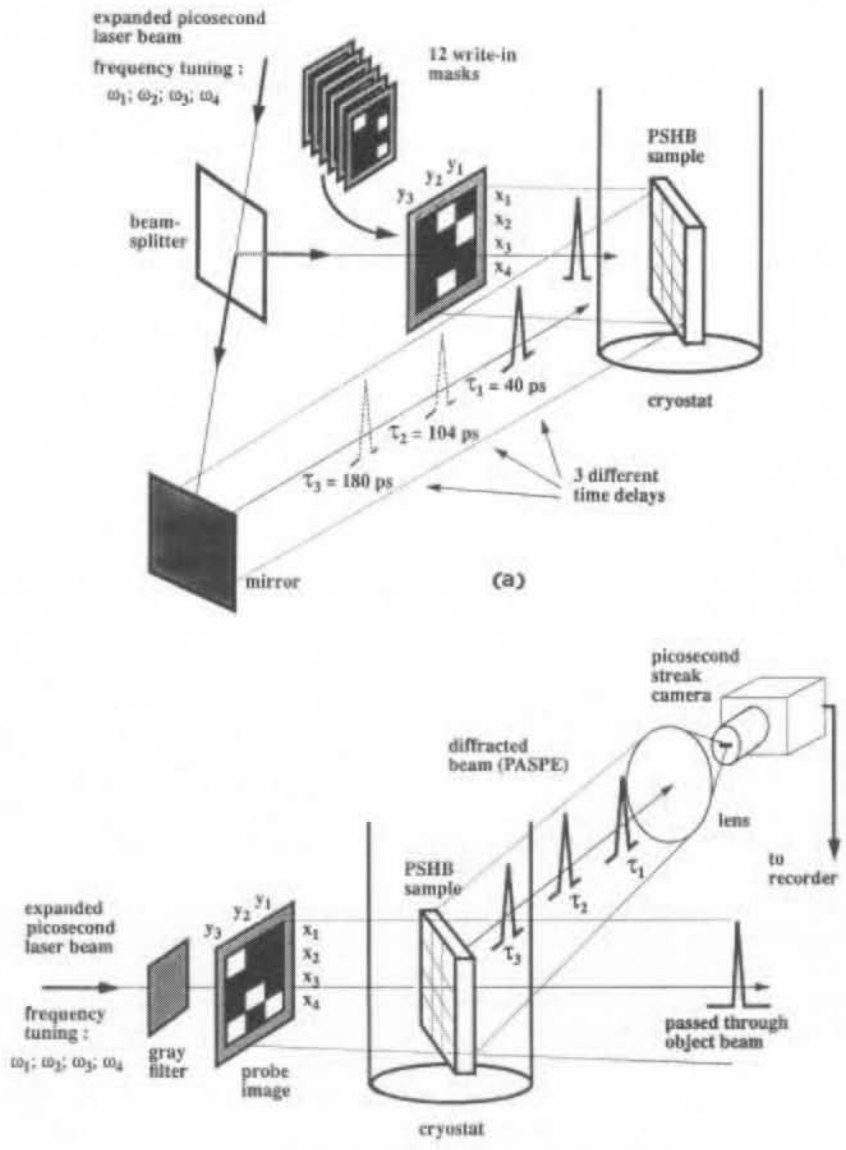

Figure 4 (a) Setup of experiment 2 and scheme of memory matrix write-in. (b) Read-out scheme of experiment 2.

The holographic scheme has the essential advantage of reduced background noise level in the readout, which makes the thresholding procedure trivial, as clearly displayed in Fig. 5. However, it requires more complicated memory writing procedure, and the PASPE holography consumes considerable space in the frequency domain (up to $10\,cm^{-1}$), equal to the space for 10^2 to 10^3 narrow spectral holes.

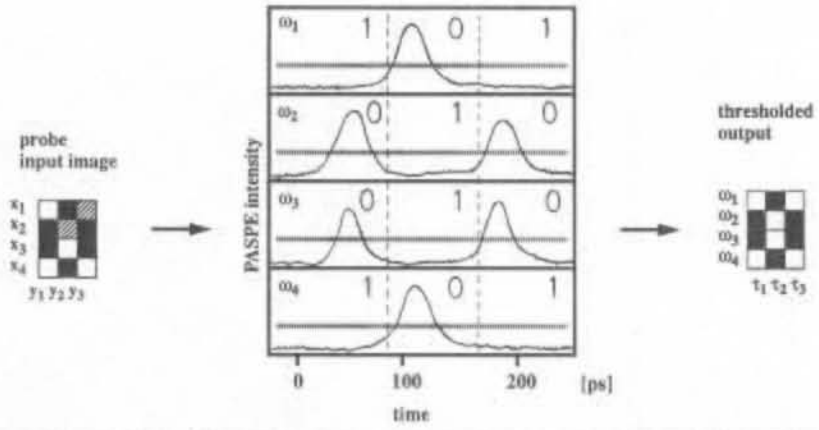

Figure 5 Results of experiment 2. The input probe image comprises two error bits (shaded squares). PASPE signal intensity is measured with streak camera at four different laser frequencies. The dashed line indicates the threshold level. Relative PASPE signal intensity above the threshold level gives bit value 0, signal below the threshold gives value 1. Memory output coincides with the original information vector $\boldsymbol{V}^{(1)}$.

4.3. Third experiment

The motivation is to demonstrate one more choice of the set of coordinates, and another mathematical algorithm, and to show the possibility of considerably increasing the number of interconnections; $32 \times 32 \times 32 = 32\,768$ interconnections are implemented. The background illumination passed through is considerably stronger than in the first experiment and to suppress it stationary holography is used to store and read out the spatial picture at each frequency [25, 26].

We use the following four 32-bit vectors:

$$\begin{aligned}
\boldsymbol{V}^{(1)} &= 1111\ 0000\ 0000\ 1111\ 1111\ 0000\ 0000\ 1111 \\
\boldsymbol{V}^{(2)} &= 1100\ 0011\ 1100\ 0011\ 1100\ 0011\ 1100\ 0011 \\
\boldsymbol{V}^{(3)} &= 0110\ 0110\ 0110\ 0110\ 0110\ 0110\ 0110\ 0110 \\
\boldsymbol{V}^{(4)} &= 1010\ 1010\ 0101\ 0101\ 1010\ 1010\ 0101\ 0101
\end{aligned} \tag{11}$$

and calculate the 3D memory tensor, T_{ijk}, following the rules (7) to (9). Figure 6 presents one out of the 32 two-dimensional 'cross-sections' of the three-dimensional memory tensor.

To materialize the interconnection matrix, three physical coordinates are used – two orthogonal spatial coordinates and frequency – where each variable has 32 different values. The scheme of the experimental arrangement is presented in Fig. 7. The expanded dye laser beam is divided into two parts by a beam-splitter At the PSHB plate the two beams (object and reference beam) cross at an angle of 10°. The path of the object beam contains a holder with an interchangeable mask. The laser beam projects the mask upon the PSHB sample so that every spatial element of the mask coincides with a corresponding spatial element of the storage plate. The reference beam possesses a plane wavefront and uniformly illuminates the whole storage area of the PSHB plate. Holograms are stored at those spatial elements (indices j and k) and frequencies (index i) for which the value of the

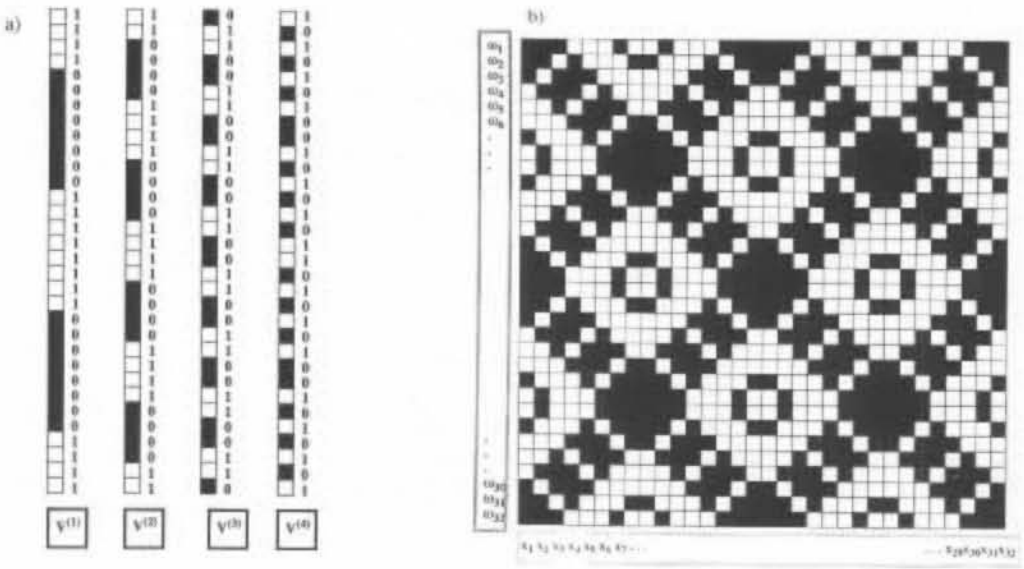

Figure 6 (a) Four information vectors and (b) one out of the 32 sections of the memory matrix in experiment 3. Black squares correspond to zero elements, white squares correspond to nonzero elements.

corresponding memory element, T_{ijk}, is not zero. Only at these positions is the write-in mask transparent to the illuminating object laser beam; at all other positions the mask is opaque and no holograms are recorded. The exposure procedure is carried out for each of the 32 frequencies by tuning the dye laser sequentially to 32 fixed frequency positions defined by an intracavity etalon.

As already mentioned above, in this case we deal with stationary PSHB holograms [25] and a simple photomultiplier or photodiode (instead of streak camera) is sufficient to detect diffracted light.

We interrogate our stored PSHB memory with four different probe vectors, each of which resembles one of the four stored vectors but contains four error bits. During the read-out the object beam is attenuated in order to avoid erasing of the memory by further hole-burning. The reference beam is blocked. To represent the probe vector we prepare a 32×32-element mask with transparent and opaque elements that correspond to the self-product of the probe vector. We place the mask in the object beam exactly at the position where before we had the memory write-in masks. At the output of the memory we have a focusing lens that collects the light diffracted from different spatial elements of the PSHB hologram onto the cathode of a photomultiplier. The passed-through read-out beam is blocked. Only the diffracted beam reaches the photomultiplier input.

The spatially integrated relative diffraction efficiency of the hologram is measured at the 32 pre-fixed frequencies of the dye laser; results are presented in Fig. 8. For three out of four probe vectors the memory output gives the correct answer – the sequence of bits obtained after thresholding of the diffraction signal reproduces a corresponding stored vector that is the closest match to the probe vector.

A shortcoming of our present experimental arrangement is that there is parasitic stray light resulting from diffraction of the read-out beam from the edges of the mask elements. The level of stray light depends on the actual mask pattern and is largest for the fourth

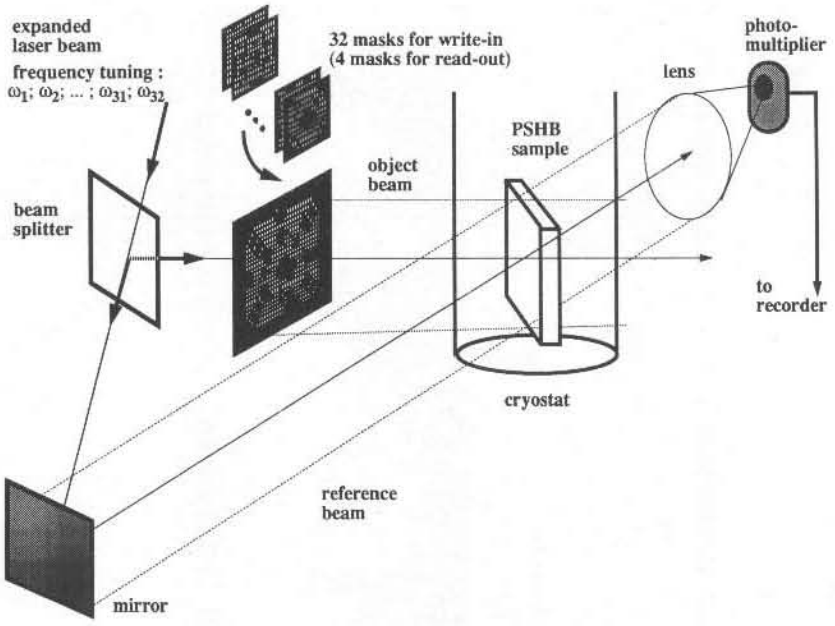

Figure 7 Scheme of experiment 3. The memorized information consists of 32 basic vectors. 32 different masks, each consisting of 32 × 32 pixels, are used to write in the 32 × 32 × 32-element memory matrix. Four different 32 × 32 masks are probed as the input, each containing four error bits (as compared to the closest matching basic vector). Three of them are corrected successfully at the output (see also Fig. 8).

probe vector. This is the reason why the recollection of the last memorized vector fails (Fig. 8d). This problem could be avoided by more careful design of the optical scheme.

From the point of view of further increasing the number of interconnects in the frequency and time dimensions in experiments 2 and 3, it is important to study the interaction between the holograms in the frequency domain [25]. The principal ways to control this interaction and to increase the storage capacity/diffraction efficiency of hole-burning holograms were discussed recently in [26].

In principle, the read-out detection of frequency-domain bits in all three experiments can also be accomplished in parallel. The trivial possibility is to use broad-band illumination and a monochromator at the output. It is also possible to use the PSHB medium itself to perform the spectral analysis of the signals, since it has much higher spectral resolution than conventional grating monochromators [12, 27]. For example, if in the write-in procedure described above the exposures at different frequencies are also carried out with different angles between the object and the reference beam, while keeping the incidence angle of the object beam constant, then the read-out of the memory with a spectrally broad laser beam comprising all the frequencies involved in write-in will give an output signal in which the different frequency components are already separated by the angle of diffraction.

5. Conclusions

We have demonstrated new possibilities of optical data storage and processing in the neural network scheme by making use of persistent spectral hole-burning. At liquid-helium temperatures hole-burning materials have very high spectral selectivity – thousands of frequencies ('different colours') may be discriminated in storage and recall.

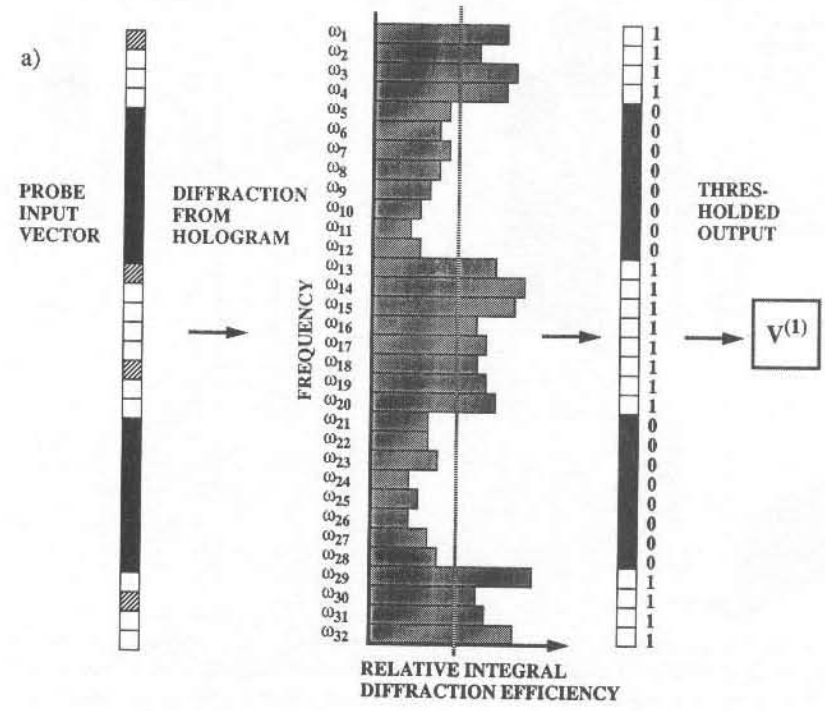
a)
PROBE INPUT VECTOR
DIFFRACTION FROM HOLOGRAM
FREQUENCY
THRES-HOLDED OUTPUT
V(1)
RELATIVE INTEGRAL DIFFRACTION EFFICIENCY

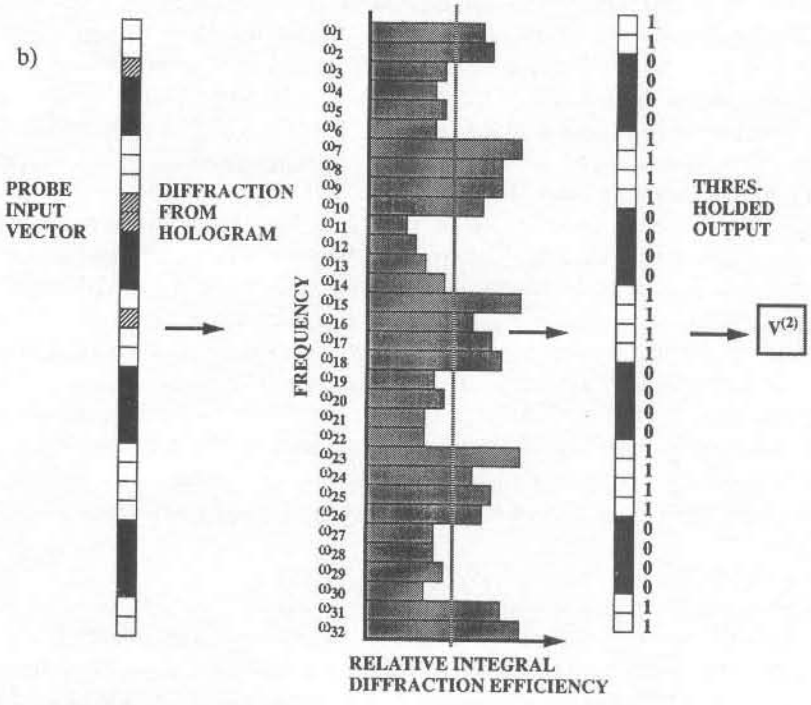
b)
PROBE INPUT VECTOR
DIFFRACTION FROM HOLOGRAM
FREQUENCY
THRES-HOLDED OUTPUT
V(2)
RELATIVE INTEGRAL DIFFRACTION EFFICIENCY

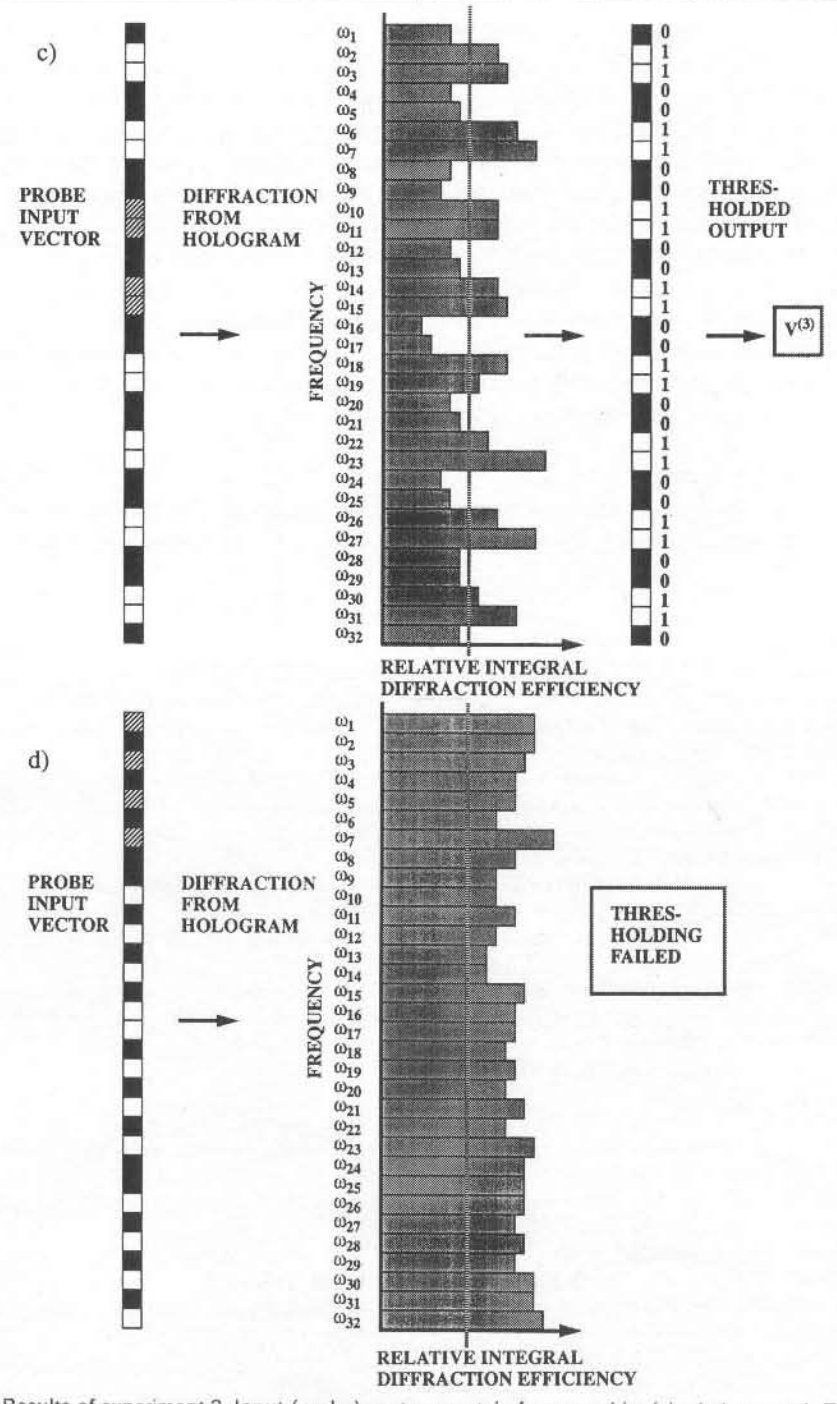

Figure 8 Results of experiment 3. Input (probe) vectors contain four error bits (shaded squares). The dashed line indicates the threshold level. Spatially integrated hologram diffraction signal above threshold level gives bit value 1, signal below threshold gives value 0. In cases (a), (b) and (c) the memory recognizes correct information vectors; in case (d) the associative recall fails owing to high background stray light, caused by diffraction at the edges of the mask in the write-in and read-out procedures.

Preparation of a persistent spectral hole-burning space- and frequency-domain filter for an associative memory with capacity to recognize images and correct errors is a time-consuming enterprise — the write-in takes up to 30 minutes. On the other hand, once properly prepared, it can be used numerous times to perform all-optical parallel multiplications of multidimensional matrices and so provide very fast service, including the conversion of input information into data encoded in frequency. The last might be helpful for transmission of data along optical fibres. We believe that this opens new horizons for increasing by several orders of magnitude the number of interconnections in an optical associative memory, which in turn should help to improve the overall performance of optical neural networks. Note also that if photon-gated (two-colour hole-burning) PSHB materials are used, rather high reading illumination intensities can be applied without erasing the memory. In this case, read-out (and optical multiplication of multielement vectors and matrices!) may be performed in fractions of a second.

Acknowledgement

Authors thank Dr Indrek Renge for chemical preparation of the PSHB samples. This work was supported, in part, by a Soros Foundation Grant awarded by the American Physical Society.

References

1. A. A. GOROKHOVSKII, R. K. KAARLI and L. A. REBANE, *JETP Lett.* **29** (1974) 216.
2. B. M. KHARLAMOV, R. I. PERSONOV and L. A. BYKOVSKAYA, *Opt. Commun.* **12** (1974) 191.
3. W. E. MOERNER, editor, *Persistent Spectral Hole Burning: Science and Applications* (Springer-Verlag, Berlin, Heidelberg, 1988) and refs. therein.
4. E. D. TRIFONOV, *Doklady Akademii Nauk SSSR* **147** (1962) 826 (in Russian).
5. K. K. REBANE, *Impurity Spectra of Solids* (Plenum Press, New York, 1970).
6. O. SILD and K. HALLER, editors, *Zero-Phonon Lines and Spectral Hole Burning in Spectroscopy and Photochemistry* (Springer-Verlag, Berlin, Heidelberg, 1988).
7. W. E. MOERNER and L. KADOR, *Phys. Rev. Lett.* **62** (1989) 2535; W. P. AMBROSE and W. E. MOERNER, *Nature* **349** (1991) 225.
8. M. ORRIT and J. BERNARD, *Phys. Rev. Lett.* **65** (1990) 2716; U. WILD, F. GÜTTLER, M. PIROTTA and A. RENN, *Chem. Phys. Lett.* **69** (1992) 1516.
9. *Technical Digest on Persistent Spectral Hole-Burning: Science and Applications*, Conference 26–28 Sept. 1991, Monterey, Calif. (Optical Society of America, Washington D.C., 1991) Vol. 16.
10. L. A. REBANE, A. A. GOROKHOVSKII and J. V. KIKAS, *Appl. Phys. B* **29** (1982) 235.
11. K. K. REBANE and L. A. REBANE, in ref. [3], p. 17.
12. J. V. KIKAS, in ref. [6] p. 89.
13. A. K. REBANE, R. K. KAARLI and P. S. SAARI, *Pis'ma Zh. Eksp. Teor. Fiz.* **38** (1983) 320 (Eng. transl. *JETP Lett.* **38** (1983) 383); A. K. REBANE, R. K. KAARLI and P. M. SAARI, *Opt. Spektrosk.* **55** (1983) 405 (Eng. transl. *Opt. Spectrosc. USSR* **55** (1983) 283); P. M. SAARI, R. K. KAARLI and A. K. REBANE, *Kvantovaya Elektron.* **12** (1985) 672 (Eng. transl. *Sov. J. Quantum Electron.* **15** (1985) 443); P. SAARI, R. KAARLI and A. REBANE, *J. Opt. Soc. Am. B* **3** (1986) 527.
14. A. REBANE, *Opt. Commun.* **65** (1988) 175.
15. N. FARHAT, D. PSALTIS, A. PRATA and E. PAEK, *Appl. Opt.* **24** (1985) 1469.
16. T. KOHONEN, *Self-Organization and Associative Memory* (Springer-Verlag, Berlin, Heidelberg, 1987).
17. J. J. HOPFIELD, *Proc. Natl Acad. Sci. USA* **79** (1982) 2554.
18. I. SHARIV and A. A. FRIESEAM, *Opt. Lett.* **14** (1989) 485.
19. J. S. JANG, S. W. JUNG, S. Y. LEE and S. Y. SHIN, *Opt. Lett.* **13** (1988) 248.
20. A. REBANE and O. OLLIKAINEN, *Opt. Commun.* **83** (1991) 246.
21. H. H. CHEN, Y. C. LEE, G. Z. SUN, H. Y. LEE, T. MAXWELL and C. L. GILES, *AIP Conf. Proc.* **151** (1986) 86.
22. D. PSALTIS and C. H. PARK, *AIP Conf. Proc.* **151** (1986) 370.
23. J. S. JANG, S. Y. SHIN and S. Y. LEE, *Opt. Lett.* **13** (1988) 693.

24. O. OLLIKAINEN, to be published in *Appl. Opt.*
25. A. RENN, A. J. MEIXNER and U. P. WILD, *J. Chem. Phys.* **92** (1990) 2748.
26. A. REBANE, S. BERNET, A. RENN and U. P. WILD, *Opt. Commun.* **86** (1991) 7; S. BERNET, B. KOHLER, A. REBANE, A. RENN and U. P. WILD, *J. Luminescence* **53** (1992) 215; S. BERNET, B. KOHLER, A. REBANE, A. RENN and U. P. WILD, *J. Opt. Soc. Am. B* **9** (1992) 987.
27. A. A. GOROKHOVSKII, J. V. KIKAS and R. V. JAANISO, USSR Patent 1312456 (1987).